

# Ultra-low-cost ‘paper-and-pencil’ device for electrically controlled micromixing of analytes

Ranabir Dey · Shantimoy Kar · Sumit Joshi ·  
Tapas K. Maiti · Suman Chakraborty

Received: 13 October 2014 / Accepted: 13 February 2015 / Published online: 24 February 2015  
© Springer-Verlag Berlin Heidelberg 2015

**Abstract** We demonstrate here a frugal, printing-based fabrication methodology for paper channels, in an effort towards developing an inexpensive micromixing device. The proposed fabrication methodology utilizes the normal ink-jet cartridge ink to create the barriers for the paper channels, without involving any additional complex materials or intermediary ink modification steps. We show through experimental observations, and pertinent scaling analysis, that the electrokinetic effects, along with the capillary and viscous forces, play a significant role in enhancing the liquid transport rate through such a paper channel under an applied electrical potential, in comparison with that observed due to natural imbibition. Thereafter, we delineate the modality of active electrical control of mixing of two liquids in such a printed ‘zigzag’ ‘paper-and-pencil’ device, by exploiting the interplay between the electrohydrodynamic flows stemming from the electrokinetic

phenomena and the specific channel geometry. The electrokinetically mediated flow of the liquid samples through the ‘zigzag’ paper channel can be judiciously controlled to either appreciably enhance the mixing characteristics or artificially maintain the segregation of the liquid streams by overriding the inherent wicking action-driven mixing within the paper matrix. Hence, the present endeavour will usher in a new generation of paper microfluidic platforms for micromixing, with enhanced production feasibility, controllability, functioning efficiency, and multiplexing capability.

**Keywords** ‘Paper-and-pencil’ devices · Paper microfluidics · Electrokinetics · Paper-based mixing · Hue-based technique

---

Ranabir Dey and Shantimoy Kar have contributed equally to this work.

**Electronic supplementary material** The online version of this article (doi:[10.1007/s10404-015-1567-3](https://doi.org/10.1007/s10404-015-1567-3)) contains supplementary material, which is available to authorized users.

---

R. Dey · S. Joshi · S. Chakraborty (✉)  
Department of Mechanical Engineering,  
Indian Institute of Technology, Kharagpur 721302, India  
e-mail: [suman@mech.iitkgp.ernet.in](mailto:suman@mech.iitkgp.ernet.in)

S. Kar · T. K. Maiti · S. Chakraborty  
Advanced Technology Development Centre,  
Indian Institute of Technology, Kharagpur 721302, India  
e-mail: [tkmaiti@hijli.iitkgp.ernet.in](mailto:tkmaiti@hijli.iitkgp.ernet.in)

T. K. Maiti  
Department of Biotechnology, Indian Institute of Technology,  
Kharagpur 721302, India

## 1 Introduction

Paper-based microfluidic devices constitute the ‘holy grail’ of microdevices, which are functionally efficient, and yet, have strikingly simple fabrication procedures (Mace and Deraney 2013). More specifically, intricate two-dimensional (Martinez et al. 2007, 2008b) and three-dimensional (Li and Liu 2014; Martinez et al. 2008a) channel geometries can be efficiently fabricated with paper substrates, in a cost-effective manner, for a wide variety of interdisciplinary applications. Presently, the applications of paper microfluidics encompass the varied fields of biomedical engineering (Chen et al. 2014; Gubala et al. 2012; Matsuura et al. 2014; Yetisen et al. 2013), flexible and disposable electronics (Kim and Steckl 2010; Kurra et al. 2013; Kurra and Kulkarni 2013), digital microfluidics (Abadian Arash 2014), energy generation (Arun et al. 2014; Thom et al. 2012), and sensors (Yoon et al. 2013), only to name a few. Moreover,

diverse efforts are also being made to alter the inherently hydrophilic nature of paper substrates to further broaden the utilitarian scope of paper-based devices (Li et al. 2013; Sousa and Mano 2013). However, the revolutionary aspect of paper microfluidics unarguably lies in its ingenious capacity to provide cost-effective, self-contained and reliable medical diagnostics in severely resource-limited setups (Ballerini et al. 2012; Chan et al. 2013; Lafleur et al. 2012; Martinez et al. 2010). The efficacy of most of these paper-based medical diagnostic applications, such as ELISA-based pathogen detection (Cheng et al. 2010; Jokerst et al. 2012), detection of heavy metal ions (Gu et al. 2011; Zhang et al. 2013), and detection of bioanalytes (Dungchai et al. 2010; Rattanarat et al. 2012), as well as the functionality of certain other combinatorial chemistry applications (Dungchai et al. 2009; Nie et al. 2010), are intrinsically dependent on the mixing efficiency of two fluids within the paper-fibre matrix. However, the natural capillarity-driven liquid transport through the prefixed paper-fibre arrangement, and consequently, the associated passive mixing dynamics, is non-controllable and generally has poor repeatability. In this regard, diverse efforts were directed to first control the liquid transport through paper microfluidic devices by external forcing mechanisms, such as surface acoustic waves (Rezk et al. 2012) and centrifugal force (on rotating platforms) (Godino and Vereshchagina 2014; Hwang et al. 2011). More recently, we have demonstrated the modality of utilizing the spontaneous, interfacial electrokinetic phenomena in paper substrates to achieve active electrical control over liquid transport in a novel, yet simple, ‘paper-and-pencil’ device (Mandal et al. 2012). However, the important aspect of characterizing the mixing performance, which is directly responsible for the functionality of majority of the paper-based microdevices, associated with such external electrical forcing mechanism still remain unaddressed.

In the present work, we first demonstrate an alternative, ultra-low-cost, printing-based fabrication methodology for ‘paper-and-pencil’ devices, which is cheaper, flexible, and more conducive for easier batch-processing in resource-limited areas than the existing fabrication procedures. Thereafter, we delineate the electrically controlled flow and associated mixing characteristics of two dyed solutions in the printed ‘paper-and-pencil’ microfluidic device. The electrically mediated flow of the dyed solutions through the paper channel is dependent on the electrokinetic phenomena, which in turn is dependent on the cellulose surface electrochemistry. The electrically mediated mixing characteristics result from the combined interplay of the channel geometry and the electrokinetic flow of the involved solutions. We believe that the present endeavour will be instrumental in establishing a yet unexplored operational paradigm for paper-based devices, in a myriad of applications, by detailing the electrically controlled mixing methodology in such devices.

## 2 Experimental section

### 2.1 Fabrication of the ‘paper-and-pencil’ microdevice

The paper channels are fabricated on Whatman® (Grade-4) cellulose paper [mean pore diameter ( $2r_m$ ): 20–25  $\mu\text{m}$ ; porosity 42 %, ‘course’] by a simple, ink-jet printing-based procedure, standardized by us. The proposed fabrication methodology directly utilizes the ink-jet cartridge ink for fabricating the barriers of the paper channels. Hence, the proposed technique is much simpler to execute for rapid prototyping, and definitely more cost-effective, than other printing-based fabrication processes for paper devices, percolated in the literature so far, like wax-printing (Carrilho et al. 2009; Lu et al. 2009, 2010) or printing of other synthesized complex substances to create the necessary barriers (Chen et al. 2013; Martinez et al. 2007). It must be noted here that very recently, a similar methodology for fabricating paper channels has been also established by using the ink of permanent markers (Xu et al. 2015). In our methodology, the design of the channel, to be used, is printed on both sides of the paper substrate by an ink-jet printer (HP Colour LaserJet 2600n), using commercially available ink. The pattern-printed paper is then heated on a hot plate at 200 °C for 4–5 min. During the heating process, the printer toner particles, deposited over both the paper surfaces, melt and penetrate through the paper pores, thereby blocking these to create a well-defined hydrophobic barrier spanning across the paper thickness. This ‘printed’ hydrophobic barrier guides the test liquid along the desired geometry of the paper channel. The proposed fabrication procedure is detailed through a flow diagram in Fig. 1.

For the present mixing study, a ‘zigzag’ paper channel, with ‘Y’-inlet junction, is fabricated following the aforementioned procedure, while the electrodes are simply ‘sketched’ on the printed paper channel by rubbing HB pencil at the designated places, as depicted in Fig. 2. Subsequently, thin copper wires are attached to the ‘pencil-sketched’ electrodes by conductive silver paste (Alfa Aesar: sheet resistance <0.025  $\Omega/\text{square}$  @ 0.001 in. thick). The necessary electric field is applied by a DC power supply (Keithley 2410 1100 V sourcemeter) connected to these copper wires.

### 2.2 Experimental procedure

In order to highlight the unique features of the mixing characteristics associated with the electrically mediated flow, mixing performances are studied, in the ‘paper-and-pencil’ device, both without the applied electrical potential ( $V$ ) and under varying magnitudes of the external electric field. For the mixing studies, two differently coloured aqueous

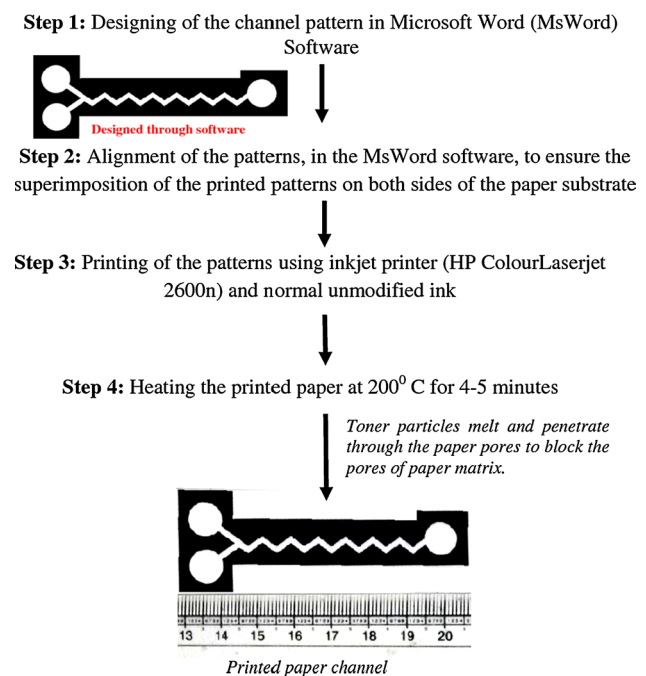


**Fig. 1** Flow diagram elucidating the fabrication procedure of the paper channel on Whatman<sup>®</sup> (Grade-4) filter paper, by the ink-jet printing method. Electrodes are sketched on the circular pads of the paper channel, by rubbing normal HB pencil

solutions of 1 mM KCl (1 mM KCl solutions stained by a red food dye in one case, and blue ink in the other, in the same volume ratio of 10:1) are dispensed on the two electrode pads at the ‘Y-inlet’ junction of the wetted paper channel. The solutions are then allowed to mix along the channel by inherent wicking action through the paper pores in one case and by electrically aided flow in the other cases. For the electrokinetically mediated mixing, the two dyed electrolyte solutions are dispensed on the electrode pads, at the Y-inlet junction, and the electrical potential is applied across the channel (as shown in Fig. 2), in tandem. The resulting flow speed is evaluated by determining the time of arrival of the dyed liquid front at the different sharp corners (as marked in Fig. 2), along the length of the ‘zigzag’ channel, from images grabbed at regular time intervals by a digital camera (Nikon COOLPIX L810).

2.3 Analysis of mixing characteristics

The associated mixing performance is quantified, from the captured images, by a colour hue-based technique (Rezk et al. 2012). In this technique, the normalized hue value of a colour image pixel is defined as  $\bar{H} = 1 - |(H - H_{mix}) / (H_b - H_{mix})|$ , where  $H$  is the actual hue value of the pixel,  $H_b$  is the hue of the blue ink-stained solution, and  $H_{mix} = (H_b + H_r) / 2$  is the hue of the colour obtained by mixing of the blue- and red-dyed

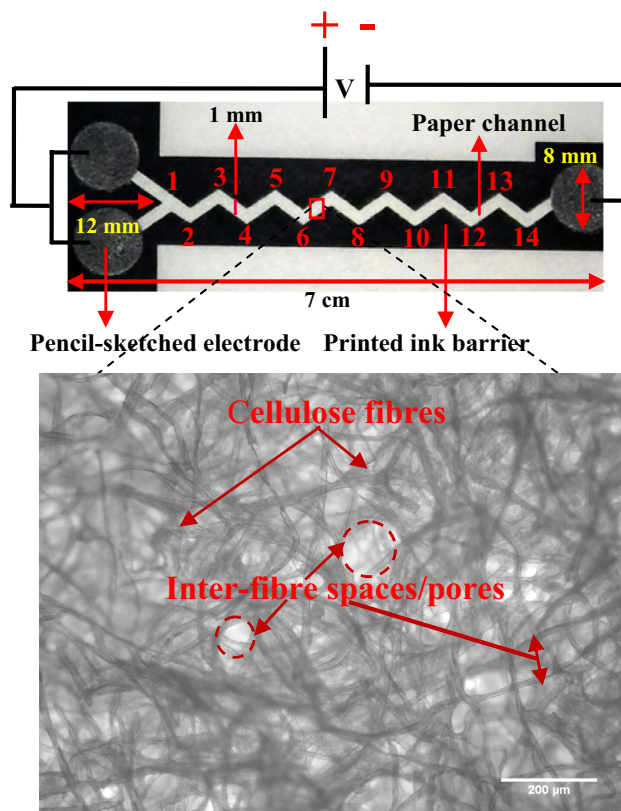


**Fig. 2** Printed ‘paper-and-pencil’ device with the ‘zigzag’ channel. The blow-up shows the microscopy image of the paper matrix [Whatman<sup>®</sup> (Grade-4) cellulose paper]. The paper structure consists of random distribution of cellulose fibres [see the microscopy image captured by an inverted microscope (Olympus IX71)], resulting in the formation of directionally non-uniform, microscopic inter-fibre spaces, or pores for liquid flow

(hue value:  $H_r = 350$ ) solutions in equal amounts and concentrations. Hence, in case of poor mixing,  $H \approx H_b$ , and consequently,  $\bar{H} \approx 0$ ; while for perfect mixing,  $H \approx H_{mix}$ , and accordingly,  $\bar{H} \approx 1$ . The mixing index is subsequently defined, over an area enclosed by  $9 \times 30$  pixels (which covers the channel width:  $w = 1$  mm), as  $\sigma = (\sum_{\text{No. of pixels}} \bar{H}) / \text{No. of pixels}$ , where  $\sigma$  always lies between 0 (no mixing) and 1 (perfect mixing). It must be noted here that we have deliberately avoided the classical fluorescence-based quantitative visualization technique for characterizing the mixing efficiency, since the present colour hue-based technique is well suited for quantifying colorimetric detection of analytes, as implemented in majority of the paper-device-based applications (like rapid diagnostic tests) (Alkasir et al. 2012; Jokerst et al. 2012), with minimalist infrastructure, unlike the fluorescence-based procedure. Hence, the present methodology can be adapted for automated analysis of test results, from paper-based devices, even in remote locations using cell phones.

### 3 Results and discussions

The paper (cellulose) fibres, in physical contact with the aqueous electrolyte solution, develop surface charge primarily due to the ionization of various functional groups (like carboxylic groups) within the cellulosic fibres (Hubbe 2006). The resulting average surface potential ( $\zeta$ -potential) of the paper channel, in contact with the 1 mM KCl solution (pH 5.5), is measured to be  $\zeta_s = -8.766 \pm 0.7813$  mV (SurPASS electrokinetic analyser for solid surfaces; Anton Paar GmbH). It must be noted here that this experimentally measured value of the  $\zeta$ -potential of the ‘zigzag’ paper channel surface is comparable to the value of  $\zeta$ -potential of flat cellulose surfaces reported in the literature (Nigmatullin et al. 2004). The surface ionization process, and the consequential development of the surface potential, triggers the spontaneous redistribution of the oppositely charged ions (cations), within the electrolyte solution, to form the electric double layer (EDL) in the immediate vicinity of the fibre surfaces (Hubbe 2006; Probst 1994). Now, on application of the external electrical potential, the free charge in the developed EDL generates an electrical body force which induces the bulk electroosmotic (Probst 1994) transport of the electrolyte solution in the direction of the applied field. However, it is instructive to note here that bulk conductivity measurements, performed by us, reveal that the molecules of both the dyes, used for staining the electrolyte solution, are charged. Hence in general, the observed motion of the dyed liquid front, under an imposed electrical field, is a culmination of the combined effects of the bulk electroosmotic flow of the electrolyte and the electrophoretic motion (Probst 1994) of the dye molecules. Accordingly, the observed electrically modulated motion of the dyed liquid front is generally referred to here as an electrokinetically mediated flow, which encompasses both the underlying electroosmotic and the electrophoretic effects. On application of the external electrical potential, the aforementioned electrokinetic effects, in conjunction with capillary and viscous forces, trigger enhanced (overall) transport of the dyed solutions, from the reservoir pads, in comparison with that observed with only normal imbibition under the no-voltage conditions (0 V), as can be clearly inferred from Fig. 3a. The displacement ( $x$ ) versus time ( $t$ ) characteristics, depicted in Fig. 3a, prove the superior liquid transport rate and controllability of the electrokinetically aided flow of the dyed solutions through the ‘zigzag’ paper channel. The electrical flow controllability stems from the fact that the additional electrical driving force, which is proportional to the external electric field strength ( $E \sim V/L$  where  $L$  is the length of the channel across which  $V$  is applied) (Chakraborty 2007; Probst 1994), results in progressively higher average dyed-liquid front speed ( $U = dx/dt$ ) at the sharp corners, with increasing

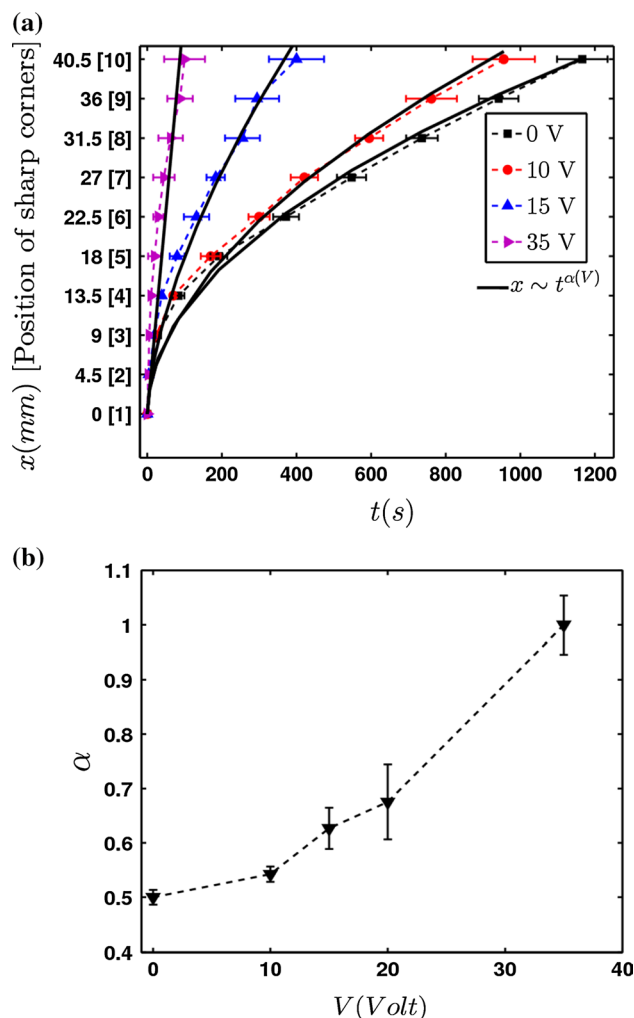


**Fig. 3** **a** Experimental observations showing the temporal variations of the displacement of the dyed liquid front, through the printed ‘zigzag’ paper channel, without electrical effects (0 V), and during electrically mediated flow under varying magnitudes of the applied electrical potential. The ordinate shows the number of the sharp corners, within parenthesis, corresponding to the actual distance along the channel. The displacement versus time characteristics approximately obey a power-law of the form:  $x \sim t^{\alpha(V)}$  (shown with solid black line). The displacement characteristics corresponding to 20 V is not shown here to maintain clarity. The data shown here represent the average values obtained from six sets of repeated experiments. The error bars represent the corresponding standard deviations of the experimental results. **b** Variation of the power-law exponent with increasing magnitude of the applied electrical potential

magnitude of the applied electrical potential. This progressive enhancement in  $U$  at the different sharp bends along the length of the channel, with increasing magnitude of  $V$ , can be easily inferred from Fig. 3a. It must be noted here that by ‘controllability’, we mean the ability to externally control/alter the liquid transport characteristics through the paper channel by the judicious control of the externally applied electrical potential. In that regard, it is quite



apparent that it is not possible to actively ‘control/alter’ the natural imbibition (without any electrical effects) through the paper channel. However, the reproducibility/repeatability of the electrically mediated flow, as quantified by the extent of the error bars, is comparable to that observed under no-voltage condition. It must be further noted here that the experimentally obtained displacement versus time characteristics, for the dyed electrolyte solution filling the paper channel, approximately conform to a power-law behaviour of the form:  $x \sim t^\alpha$  (see Fig. 3a). For  $V = 0$  V, we obtain  $\alpha = 0.5$  (see Fig. 3b), and accordingly, it follows that  $x \sim t^{0.5}$  for 0 V. Therefore, under the no-voltage condition, the observed transport dynamics of the liquid through the paper channel adhere to the classical Washburn regime (Masoodi and Pillai 2010), stemming from the balance between the capillary and viscous forces. However, under an applied electrical potential, the value of the power-law exponent ( $\alpha$ ) deviates from 0.5. More specifically, the value of  $\alpha$  progressively increases with increasing magnitude of  $V$  (see Fig. 3b), which embodies the enhanced rate of liquid transport due to the additional electrical effects. Interestingly, for large magnitude of the applied electrical potential (e.g.  $V = 35$  V)  $\alpha \sim 1$  (see Fig. 3b), and accordingly, we obtain  $x \sim t$ , which suitably describes the experimentally observed displacement characteristics at higher values of  $V$  (see the  $x$  vs.  $t$  characteristics for 35 V in Fig. 3a). It can be shown that such linear relation between  $x$  and  $t$  follows directly from the dominant balance between the viscous force ( $\mu x U \sim \mu x \left(\frac{dx}{dt}\right)$ ) and the electrical body force ( $\rho_c E \sim \varepsilon \zeta_s A V x / \lambda_D^2 L$ ):  $U = \frac{dx}{dt} \sim \left(\frac{\varepsilon \zeta_s A V}{\mu \lambda_D^2 L}\right)$ , during the liquid transport through the paper channel under large magnitudes of the applied electrical potential. Here,  $\mu$  is the viscosity of the liquid,  $\rho_c$  is the total free charge in the liquid volume inside the paper channel consistent with the classical electrokinetic description (Probstein 1994),  $\varepsilon$  is the absolute permittivity of the electrolyte solution,  $A$  is a reference area scale consistent with the developed EDL, and  $\lambda_D$  is the reference length scale [Debye length; approximately equal to 9.7 nm for 1 mM KCl (Probstein 1994)] for the EDL. From the aforementioned linear scaling relation, and by using the displacement characteristics corresponding to 35 V (for specifying  $x$  and  $t$ ), the order of magnitude of the surface potential of the paper channel can be also theoretically estimated as  $O(\zeta_s) \sim \frac{\mu \lambda_D^2 L}{\varepsilon A V} \times O\left(\frac{dx}{dt}\right) \sim 9.95$  mV. This theoretical estimation of  $\zeta_s$  is in good agreement with the independently measured value of the average surface potential ( $-8.766 \pm 0.7813$  mV), as mentioned previously. The good coherence between the theoretical value of  $\zeta_s$  for the paper channel surface obtained from the scaling estimate and the experimentally measured value of the same further validates the fact that the observed transport of the

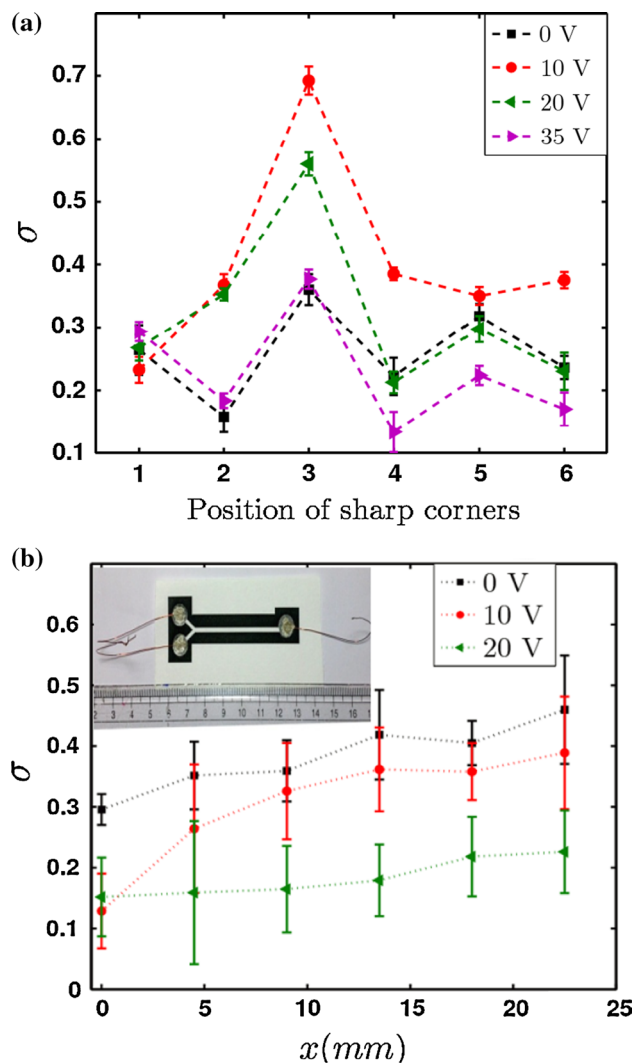


**Fig. 4** **a** Comparison of the mixing performance of the blue- and red-dyed solutions, at the sharp bends along the ‘zigzag’ paper channel, with Y-inlet junction, in the absence of any electrical effect (0 V) and under electrically controlled flows of the same. **b** Mixing performance (analysed by the same hue-based technique) of identical, dyed solutions, along the length of a straight paper channel, with Y-inlet junction, of identical width, in the absence of any electrical effect (0 V) and under electrokinetically mediated flows of the same (at 10 and 20 V). The ‘paper-and-pencil’ device with the straight channel, fabricated by the same ink-jet printing-based procedure as discussed previously, is shown in the *inset*. The data shown here (in both **a** and **b**) represent the average values obtained from six sets of repeated experiments. The *error bars* represent the standard deviations of the experimental results

dyed solution through the ‘zigzag’ paper channel, under an applied electrical potential, is indeed electrokinetically mediated. Now, the important question that remains to be addressed is how does such electrically controlled flow (as shown in Fig. 3) alters the mixing characteristics of the dyed solutions in the paper channel?

To address the aforementioned question, Fig. 4a delineates the mixing performance, as represented by the mixing index ( $\sigma$ ) at the different sharp bends of the ‘zigzag’ paper channel, associated with both flows with and without (0 V) electrical effects. It is to be first noted here that the passive mixing of the two dyed solutions, as being discussed here, is solely diffusion-driven, in the absence of random velocity fluctuations for the low Reynolds number ( $O(\text{Re}) \sim (U_w)/\nu \sim 10^{-2} - 1$ , where  $\nu$  is the liquid kinematic viscosity) regimes under consideration. Now, for the paper channel, the inherent random paper–fibre arrangement forms a matrix of directionally non-uniform inter-fibre spaces or pores (see the blow-up in Fig. 2), which results in locally non-uniform liquid transport. Such locally non-uniform liquid transport facilitates the interspersions of the initially segregated liquid streams, and hence, inherently facilitates the diffusion-driven mixing. When such flow of two dyed solutions through the paper matrix occurs in the absence of any external electrical potential, it results in a maximum mixing index of 0.36 (or 36 %), at bend no. 3 (see Fig. 4a), corresponding to a Péclet number of  $\text{Pe} = (U_w)/D \sim 182.1$  (where  $D \sim 10^{-9} \text{ m}^2/\text{s}$  (Chen and Yang 2007; Rezk et al. 2012) is the diffusion coefficient). Here, the Péclet number, corresponding to a particular bend, is estimated by utilizing the average speed ( $U$ ) at which the dyed liquid front arrives at that bend (i.e. bend no. 3 here), as evaluated from the displacement characteristics depicted in Fig. 3a. The average dyed–liquid front speed controls the advective transport of the liquid, and hence, dictates the relative strengths of advective to diffusive transport of the dyed liquid as quantified by Pe. Consequently,  $U$ , and accordingly Pe at a particular bend, plays an underlying role in influencing the associated mixing strength at that bend. Apparently, the mixing characteristics depicted in Fig. 4a indicate that the mixing performance is generally poorer at the even-numbered sharp bends (2, 4, 6), compared with the odd-numbered ones (3, 5). This is due to the specific (asymmetric) design of the sharp bends relative to the outlet branch of the Y-inlet junction of the ‘zigzag’ channel. Such non-uniformity in the mixing performance, at the sharp bends along the ‘zigzag’ channel, is solely a consequence of the ‘zigzag’ channel geometry, and not an artefact of the colour hue-based analysis technique. Since, such handedness effects are not observed for the mixing characteristics in a straight paper channel with Y-inlet junction, under identical conditions, as shown in Fig. 4b. The variation of  $\sigma$  for the straight paper channel, with Y-inlet junction, as observed in Fig. 4b, is in accordance with the classical understanding of the mixing phenomenon for two liquid streams, where the mixing index gradually increases along the length of the channel. Moreover, in the straight paper channel, the mixing index at a definite axial location along the paper channel progressively

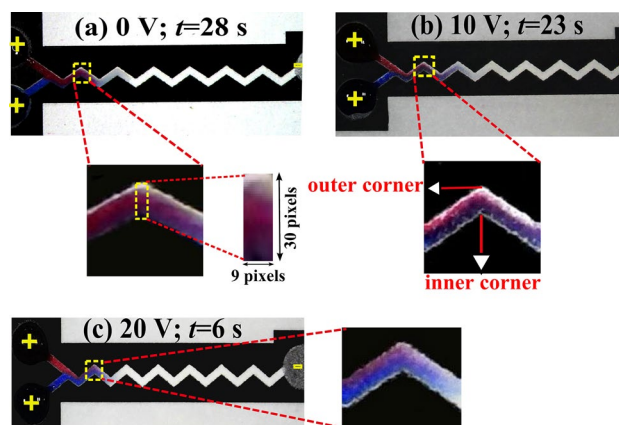


**Fig. 5** Real-time images capturing the final mixing performance, at sharp corner no. 3, **a** without any electrical effects, **b** during electrokinetically aided flow of the dyed solutions through the channel at 10 V, and **c** during electrokinetically mediated flow of the dyed solutions at 20 V

decreases with increasing magnitude of the applied electrical potential (i.e. for 10 and 20 V), as compared to that observed under the no-voltage condition (see Fig. 4b). The decreasing value of the mixing index, with increasing magnitude of  $V$ , simply highlights the progressive reduction in the diffusion-driven mixing triggered by the increasing rate of advective liquid transport, due to the involved electrokinetic phenomena under an applied electrical potential (as discussed in relation to Fig. 3). It must be noted here that the zigzag geometry imposed handedness effects, as discussed here, are also documented in the literature (Rezk et al. 2012). More importantly, the perceived non-uniformity in the mixing index does not hamper the clear identification of the unique features of the electrically mediated mixing characteristics through the ‘zigzag’ paper channel, compared to that observed under the no-voltage condition. Interestingly, for the electrokinetically aided flow through the identical ‘zigzag’ paper channel at 10 V, the mixing performance is appreciably enhanced ( $\sigma_{\text{max}} = 0.69$ ) at all the sharp bends (see Fig. 4a) in comparison with that observed under the no-voltage condition. Specifically, for such electrically mediated transport through the paper–fibre matrix, there is a staggering 91.6 % increase in the maximum mixing efficiency over the same length of the channel (i.e. 9 mm; bend no. 3), as compared to the mixing under 0 V, while Pe remains comparable for the two cases ( $\text{Pe} \sim 219.4$  at bend no. 3 for the electrically aided flow at 10 V). Furthermore, this enhancement in mixing is achieved over 17.8 % shorter time span, as the dyed liquid solutions reach the definite channel bend faster under additional electrical actuation due to greater flow speed. The aforementioned fact can be easily comprehended by comparing Fig. 5a and b which depicts the real-time images showing the mixing

performance, at sharp corner no. 3, without any electrical effects and under an applied electrical potential of 10 V, respectively. This enhancement in mixing primarily stems from the fact that at a sharp bend, there is a greater potential drop across the inner corner, and hence, a higher electric field strength, as compared to that across the outer corner (see Fig. 5b). This locally non-uniform electric field strength, which implies non-uniform electrical force across the bend width, sets up a relatively higher net (electrokinetically mediated) flow rate across the inner corner than that across the outer corner. The culminating ‘racetrack effect’ (Chen and Yang 2007) stretches a liquid volume, consisting of the two dyed streams. This stretching of the liquid volume increases the interfacial areas of contact between the two dyed liquid streams within the paper–fibre matrix. Such increase in the interfacial areas, due to the combined interplay of the channel geometry and the involved electrohydrodynamics, consequently enhances the molecular diffusion-driven mixing at the respective bends. However,  $\sigma$  decreases at the sharp corners (including bend no. 3) along the ‘zigzag’ channel with further increase in the electric field strength (i.e. at 20 V) (see Fig. 4a). The lower mixing efficiency, under a higher applied electrical potential, follows from the fact that the corresponding flow speed at the sharp corners (see Fig. 3a), and consequently, the associated Pe (for e.g. now Pe  $\sim$  933.9 at bend no. 3) is appreciably higher due to the additional electrokinetic effects. The higher rate of advective transport culminates in relatively reduced liquid residence time at a particular bend. Such decreased time of contact between the two liquid streams reduces the diffusion-driven mixing between the dyed solutions in comparison with that observed at 10 V. This is further substantiated by the real-time image in Fig. 5c which captures the poor mixing of the blue- and red-dyed solutions at sharp corner no. 3 under 20 V (the blue dye remains almost blue near the inner corner). Furthermore, the fact that the blue-dyed liquid near the inner corner is almost unmixed, and is relatively advanced than the red-dyed stream, at the same time instant, reflects the aforementioned ‘racetrack’ effect, albeit more prominent at 20 V; and now, is detrimental for mixing. Such advection-driven attenuation of the mixing is further enhanced at an even higher applied electrical potential of 35 V (see Fig. 4a). At this voltage, the electrokinetically induced stronger advective effect (Pe  $\sim$  1308 at bend no. 3) further lowers the diffusion-driven mixing efficiency to an extent that it is comparable to (bend nos. 2 and 3) or even lower than (bend nos. 4, 5 and 6) that obtained with 0 V (see Fig. 4a). However, the fact that under high magnitude of the applied electrical potential, the electrically dominated faster rate of liquid transport lowers the mixing index of the liquid streams at the sharp corners, even below that observed with inherent wicking action, implies that such electrically mediated

flow can be also implemented for artificially keeping two liquid streams segregated, by superseding the inherent capillary-driven mixing tendency in paper devices, if the application demands so.

#### 4 Conclusion

We conclude here that the electrokinetic phenomena, in conjunction with the capillary and viscous effects, indeed plays a significant role in progressively enhancing the liquid flow rate through the paper channel with increasing magnitude of the applied electrical potential. We further show that the ultra-low-cost, printed ‘paper-and-pencil’ device, with the ‘zigzag’ channel, can be suitably used to achieve active electrical control over the mixing efficiency of liquid streams within the paper–fibre matrix, by exploiting the interplay of such electrokinetically aided flow and the specific channel geometry. Significant enhancement in mixing is achievable over a short device length, and over a shorter time interval, as compared to that possible with inherent wicking action, by judiciously controlling the electrokinetically mediated flow (Pe  $\leq$  220). Practical implications of such findings can be far-reaching. In essence, the modality of electrically controlled mixing in printed paper channels, as demonstrated here, will greatly augment the cost-effectiveness, freedom of design, and efficacy of paper-based analytic devices, which depend on the mixing of liquid reagents, for a myriad of applications, particularly in pathological diagnostics and analytical chemistry. Moreover, the fact that the same electrically mediated flow can be implemented for artificially maintaining segregation of liquid streams further adds to the versatility (multiplexing capability) of the device. Finally, the simplistic printing-based fabrication methodology, in conjunction with the easily integrable electrical flow control, will bring us closer to achieving the elusive goal of developing frugal, controllable, efficient, and portable microfluidic platforms for developing countries.

**Acknowledgments** Ranabir Dey and Shantimoy Kar greatly acknowledge Ms. Deepika Malpani and Mr. Prasad Gosavi from Anton Paar for facilitating the measurement of the surface potential of the paper channel by using the Electrokinetic analyser for solid surfaces (Anton Paar GmbH). Shantimoy Kar greatly acknowledges Council of Scientific and Industrial Research (CSIR), India, for his research fellowship.

#### References

- Abadian Arash SJ-A (2014) Paper-based digital microfluidics. *Microfluid Nanofluid* 16:989–995. doi:10.1007/s10404-014-1345-7
- Alkafir RSJ, Ornatska M, Andreescu S (2012) Colorimetric paper bioassay for the detection of phenolic compounds. *Anal Chem* 84(22): 9729–9737

- Arun RK, Halder S, Chanda N, Chakraborty S (2014) A paper based self-pumping and self-breathing fuel cell using pencil stroked graphite electrodes. *Lab Chip* 14(10):1661–1664. doi:[10.1039/c4lc00029c](https://doi.org/10.1039/c4lc00029c)
- Ballerini DR, Li X, Shen W (2012) Patterned paper and alternative materials as substrates for low-cost microfluidic diagnostics. *Microfluid Nanofluid* 13:769–787. doi:[10.1007/s10404-012-0999-2](https://doi.org/10.1007/s10404-012-0999-2)
- Carrilho E, Martinez AW, Whitesides GM (2009) Understanding wax printing : a simple micropatterning process for paper-based microfluidics. *Anal Chem* 81:7091–7095
- Chakraborty S (2007) Electroosmotically driven capillary transport of typical non-Newtonian biofluids in rectangular microchannels. *Anal Chim Acta* 605(2):175–184. doi:[10.1016/j.aca.2007.10.049](https://doi.org/10.1016/j.aca.2007.10.049)
- Chan CPY, Mak WC, Cheung KY, Sin KK, Yu CM, Rainer TH, Renneberg R (2013) Evidence-based point-of-care diagnostics: current status and emerging technologies. *Annu Rev Anal Chem (Palo Alto, CA)* 6:191–211. doi:[10.1146/annurev-anchem-062012-092641](https://doi.org/10.1146/annurev-anchem-062012-092641)
- Chen J-K, Yang R-J (2007) Electroosmotic flow mixing in zigzag microchannels. *Electrophoresis* 28(6):975–983. doi:[10.1002/elps.200600470](https://doi.org/10.1002/elps.200600470)
- Chen B, Kwong P, Gupta M (2013) Patterned fluoropolymer barriers for containment of organic solvents within paper-based microfluidic devices. *ACS Appl Mater Interfaces* 5:12701–12707
- Chen C, Lin B-R, Wang H-K, Fan S-T, Hsu M-Y, Cheng C-M (2014) Paper-based immunoaffinity devices for accessible isolation and characterization of extracellular vesicles. *Microfluid Nanofluid* 16(5):849–856. doi:[10.1007/s10404-014-1359-1](https://doi.org/10.1007/s10404-014-1359-1)
- Cheng C-M, Martinez AW, Gong J, Mace CR, Phillips ST, Carrilho E, Whitesides GM (2010) Paper-based ELISA. *Angew Chem Int Ed Engl* 122(28):4881–4884. doi:[10.1002/ange.201001005](https://doi.org/10.1002/ange.201001005)
- Dungchai W, Chailapakul O, Henry CS (2009) Electrochemical detection for paper-based microfluidics. *Anal Chem* 81(6):5821–5826
- Dungchai W, Chailapakul O, Henry CS (2010) Use of multiple colorimetric indicators for paper-based microfluidic devices. *Anal Chim Acta* 674(2):227–233. doi:[10.1016/j.aca.2010.06.019](https://doi.org/10.1016/j.aca.2010.06.019)
- Godino N, Vereshchagina E (2014) Centrifugal automation of a triglyceride bioassay on a low-cost hybrid paper-polymer device. *Microfluid Nanofluid* 16:895–905. doi:[10.1007/s10404-013-1283-9](https://doi.org/10.1007/s10404-013-1283-9)
- Gu Z, Zhao M, Sheng Y, Bentolila LA, Tang Y (2011) Detection of mercury ion by infrared fluorescent protein and its hydrogel-based paper assay. *Anal Chem* 83:2324–2329
- Gubala V, Harris LF, Ricco AJ, Tan MX, Williams DE (2012) Point of care diagnostics: status and future. *Anal Chem* 84(2):487–515. doi:[10.1021/ac2030199](https://doi.org/10.1021/ac2030199)
- Hubbe MA (2006) Sensing the electrokinetic potential of cellulosic fiber surfaces. *BioResources* 1(1):116–149
- Hwang H, Kim S-H, Kim T-H, Park J-K, Cho Y-K (2011) Paper on a disc: balancing the capillary-driven flow with a centrifugal force. *Lab Chip* 11(20):3404–3406. doi:[10.1039/c1lc20445a](https://doi.org/10.1039/c1lc20445a)
- Jokerst JC, Adkins JA, Bisha B, Mentele MM, Goodridge LD, Henry CS (2012) Development of a paper-based analytical device for colorimetric detection of select foodborne pathogens. *Anal Chem* 84:2900–2907
- Kim DY, Steckl AJ (2010) Electrowetting on paper for electronic paper display. *ACS Appl Mater Interfaces* 2(11):3318–3323. doi:[10.1021/am100757g](https://doi.org/10.1021/am100757g)
- Kurra N, Kulkarni GU (2013) Pencil-on-paper: electronic devices. *Lab Chip* 13(15):2866–2873. doi:[10.1039/c3lc50406a](https://doi.org/10.1039/c3lc50406a)
- Kurra N, Dutta D, Kulkarni GU (2013) Field effect transistors and RC filters from pencil-trace on paper. *Phys Chem Chem Phys* 15(21):8367–8372. doi:[10.1039/c3cp50675d](https://doi.org/10.1039/c3cp50675d)
- Lafleur L, Stevens D, McKenzie K, Ramachandran S, Spicar-Mihalic P, Singhal M, Lutz B (2012) Progress toward multiplexed sample-to-result detection in low resource settings using microfluidic immunoassay cards. *Lab Chip* 12(6):1119–1127. doi:[10.1039/c2lc20751f](https://doi.org/10.1039/c2lc20751f)
- Li X, Liu X (2014) Fabrication of three-dimensional microfluidic channels in a single layer of cellulose paper. *Microfluid Nanofluid*. doi:[10.1007/s10404-014-1340-z](https://doi.org/10.1007/s10404-014-1340-z)
- Li L, Breedveld V, Hess DW (2013) Design and fabrication of superamphiphobic paper surfaces. *ACS Appl Mater Interfaces* 5:5381–5386
- Lu Y, Shi W, Jiang L, Qin J, Lin B (2009) Rapid prototyping of paper-based microfluidics with wax for low-cost, portable bioassay. *Electrophoresis* 30(9):1497–1500. doi:[10.1002/elps.200800563](https://doi.org/10.1002/elps.200800563)
- Lu Y, Shi W, Qin J, Lin B (2010) Fabrication and characterization of paper-based microfluidics prepared in nitrocellulose membrane by wax printing. *Anal Chem* 82:935–941
- Mace CR, Deraney RN (2013) Manufacturing prototypes for paper-based diagnostic devices. *Microfluid Nanofluid* 16(5):801–809. doi:[10.1007/s10404-013-1314-6](https://doi.org/10.1007/s10404-013-1314-6)
- Mandal P, Dey R, Chakraborty S (2012) Electrokinetics with “paper-and-pencil” devices. *Lab Chip* 12(20):4026–4028. doi:[10.1039/c2lc40681k](https://doi.org/10.1039/c2lc40681k)
- Martinez AW, Phillips ST, Butte MJ, Whitesides GM (2007) Patterned paper as a platform for inexpensive, low-volume, portable bioassays. *Angew Chem Int Ed Engl* 46(8):1318–1320. doi:[10.1002/anie.200603817](https://doi.org/10.1002/anie.200603817)
- Martinez AW, Phillips ST, Whitesides GM (2008a) Three-dimensional microfluidic devices fabricated in layered paper and tape. *Proc Natl Acad Sci USA* 105(50):19606–19611. doi:[10.1073/pnas.0810903105](https://doi.org/10.1073/pnas.0810903105)
- Martinez AW, Phillips ST, Wiley BJ, Gupta M, Whitesides GM (2008b) FLASH: a rapid method for prototyping paper-based microfluidic devices. *Lab Chip* 8(12):2146–2150. doi:[10.1039/b811135a](https://doi.org/10.1039/b811135a)
- Martinez AW, Phillips ST, Whitesides GM, Carrilho E (2010) Diagnostics for the developing world: microfluidic paper-based analytical devices. *Anal Chem* 82(1):3–10. doi:[10.1021/ac9013989](https://doi.org/10.1021/ac9013989)
- Masoodi R, Pillai KM (2010) Darcy’s law-based model for wicking in paper-like swelling porous media. *Am Inst Chem Eng* 56:2257–2267. doi:[10.1002/aic](https://doi.org/10.1002/aic)
- Matsuura K, Chen K-H, Tsai C-H, Li W, Asano Y, Naruse K, Cheng C-M (2014) Paper-based diagnostic devices for evaluating the quality of human sperm. *Microfluid Nanofluid* 16(5):857–867. doi:[10.1007/s10404-014-1378-y](https://doi.org/10.1007/s10404-014-1378-y)
- Nie Z, Deiss F, Liu X, Akbulut O, Whitesides GM (2010) Integration of paper-based microfluidic devices with commercial electrochemical readers. *Lab Chip* 10(22):3163–3169. doi:[10.1039/c0lc00237b](https://doi.org/10.1039/c0lc00237b)
- Nigmatullin R, Lovitt R, Wright C, Linder M, Nakari-Setälä T, Gama M (2004) Atomic force microscopy study of cellulose surface interaction controlled by cellulose binding domains. *Colloids Surf B Biointerfaces* 35(2):125–135. doi:[10.1016/j.colsurfb.2004.02.013](https://doi.org/10.1016/j.colsurfb.2004.02.013)
- Probstein RF (1994) *Physicochemical hydrodynamics: an introduction*, 2nd edn. Wiley, New York
- Rattananat P, Dungchai W, Siangproh W, Chailapakul O, Henry CS (2012) Sodium dodecyl sulfate-modified electrochemical paper-based analytical device for determination of dopamine levels in biological samples. *Anal Chim Acta* 744:1–7. doi:[10.1016/j.aca.2012.07.003](https://doi.org/10.1016/j.aca.2012.07.003)
- Rezk AR, Qi A, Friend JR, Li WH, Yeo LY (2012) Uniform mixing in paper-based microfluidic systems using surface acoustic waves. *Lab Chip* 12(4):773–779. doi:[10.1039/c2lc21065g](https://doi.org/10.1039/c2lc21065g)
- Sousa MP, Mano JF (2013) Superhydrophobic paper in the development of disposable labware and lab-on-paper devices. *ACS Appl Mater Interfaces* 5:3731–3737
- Thom NK, Yeung K, Pillion MB, Phillips ST (2012) “Fluidic batteries” as low-cost sources of power in paper-based microfluidic devices. *Lab Chip* 12(10):1768–1770. doi:[10.1039/c2lc40126f](https://doi.org/10.1039/c2lc40126f)
- Xu C, Cai L, Zhong M, Zheng S (2015) Low-cost and rapid prototyping of microfluidic paper-based analytical devices by inkjet printing of permanent marker ink. *RSC Adv* 5:4770–4773



- Yetisen AK, Akram MS, Lowe CR (2013) Paper-based microfluidic point-of-care diagnostic devices. *Lab Chip* 13(12):2210–2251. doi:[10.1039/c3lc50169h](https://doi.org/10.1039/c3lc50169h)
- Yoon B, Shin H, Kang E, Cho DW, Shin K, Chung H (2013) Inkjet-compatible single-component polydiacetylene precursors for thermochromic paper sensors. *ACS Appl Mater Interfaces* 5:4527–4535
- Zhang M, Ge L, Ge S, Yan M, Yu J, Huang J, Liu S (2013) Three-dimensional paper-based electrochemiluminescence device for simultaneous detection of  $Pb^{2+}$  and  $Hg^{2+}$  based on potential-control technique. *Biosens Bioelectron* 41(2013):544–550. doi:[10.1016/j.bios.2012.09.022](https://doi.org/10.1016/j.bios.2012.09.022)